Articles

Structural and Biophysical Insights into the Role of the Insert Region in Rac1 Function†

Roopa Thapar,* Antoine E. Karnoub, and Sharon L. Campbell*

Department of Biochemistry and Biophysics, School of Medicine, and Lineberger Comprehensive Cancer Center, University of North Carolina at Chapel Hill, Chapel Hill, North Carolina 27599

Received November 1, 2001; Revised Manuscript Received January 15, 2002

ABSTRACT: A 13 amino acid insertion that forms a short 3_{10} helix between β-strand 5 and α-helix 4 is a distinguishing feature among most members of the Rho family of GTPases, yet the precise role of this region in signal transduction is poorly understood. Previous in vivo functional studies have implicated the insert region of RhoA, Rac1, and Cdc42 to be important for cell transformation, regulation of the actin cytoskeleton, controlling DNA synthesis, and in the activation of downstream targets. In Rac1, our recent biological studies have suggested that the insert is important for SRF activation and the formation of lamellipodia but is dispensable for all other cellular functions of this protein. In the studies reported herein, we have characterized the effect of the insert deletion on Rac1 structure, thermodynamic stability, and the kinetics of nucleotide association. These in vitro studies help clarify biological data and provide further insights as to the role of this 13 amino acid region in modulating Rac1 function. The studies reveal that deletion of the insert has no effect on Rac1 structure and causes only a marginal (∼0.8 kcal/mol) decrease in the ΔG^{fold} of Rac1·GDP·Mg^{2+}. The intrinsic rate of nucleotide dissociation of Rac1·Δ^{ins} is decreased by about 1.5-fold compared to that of wild type, and a 3-fold increase in the GEF (Vav2)-mediated exchange rate is observed. In addition, deletion of the insert does not change the K_D for the interaction of Rac1 with GDI, and similar to that previously observed for Cdc42, no inhibition of GDP dissociation is observed for the deletion mutant relative to that for the native protein. Taken together, the structural and biochemical studies reported here are consistent with our biological data reported previously and suggest that the most likely role of the insert region must be to serve as a binding interface for downstream effectors, particularly those important for actin regulation.

Rho GTPases such as RhoA, Cdc42, and Rac1 are important members of the Ras superfamily of small guanosine triphosphatases (for reviews see *1*−*5*). Rho proteins control multiple signaling pathways and play critical roles in regulating the cytoskeleton, activating gene transcription, controlling cell cycle progression, cell proliferation, and apoptosis. A unique feature of these proteins is the presence of a 13 amino acid helical "insert" between β-strand 5 and α-helix 4. In this study, we investigate the structural and thermodynamic consequences of deleting this region in the Rho family protein Rac1, and we describe how deletion of this helical insert region affects the association of Rac1 with guanine nucleotide substrates, with its regulators Vav2 and Rho-GDI, and with phospholipids. The structural and biochemical studies reported herein are done in vitro (i.e., in a cell-free system) and complement in vivo studies that were previously performed on this deletion mutant in Rac1 (*6*).

The cellular functions of small GTPases depend on their interactions with downstream effectors in a GTP-dependent manner; hence, there is considerable interest in identifying regions and residues on a GTPase that may be important for imparting specificity in signal transduction pathways. Similar to Ras, Rho proteins shuttle between an active GTP/Mg^{2+} complex and an inactive GDP/Mg^{2+}-bound state. Solution NMR and crystallographic studies (*7*−*12*) reveal that Rho GTPases share a similar overall topology with H−Ras (Figure 2), and the exchange of GDP for the activating GTP (or the GTP-mimic GMPPNP) is accompanied by a conformational change that affects two regions of the protein, namely, loop 2/β-strand 2 (Ras residues 30−38, switch I) and loop 4/α−helix 2/loop 5 (Ras residues 59−77, switch II). These regions are conserved and are functionally important for interaction of Rho proteins with GEFs, GAPs, and downstream effectors such as ACK, PAK, and NADPH oxidase.

In addition, most Rho family proteins also have a 13 amino acid insertion that forms a short, solvent-exposed, 3_{10} helix between β-strand 5 and α-helix 4. The insert region is highly charged, and residues that make up the insert differ between

† This work was supported by NIH Grant R01 CA 83943-01.

* To whom correspondence should be addressed. E-mail: thapar@email.unc.edu, campbesl@med.unc.edu. Tel: (919) 966-6781. Fax: (919) 966-2852.

10.1021/bi0120087 CCC: $22.00
Published on Web 02/28/2002

RhoA, Rac1, and Cdc42, suggesting that these residues might be involved in conferring specificity to Rho GTPase targets. In Rac1, numerous studies have sought to investigate the involvement of the insert in mediating interactions with its downstream effectors (*13*−*15*); however, as yet, none of the known Rac1 effectors has been shown to interact directly with Rac1 through the insert region. We evaluated the effect of the insert deletion on Rac1-mediated cellular signaling and transformation (*6*) and found that deletion of the insert region did not abolish the transforming activity of Rac1 but sustained ROS production in REF-52 cells and NF-kB activation in NIH3T3 cells. However, deletion of the insert region did diminish SRF activation and completely abrogated the formation of lamellipodia or membrane ruffles, which is the hallmark of Rac1 activation. These studies conflicted with previous reports on Rac1 (*15*), wherein deletion of insert residues 124−135 was found to have no effect on actin polymerization in COS1 cells but did abrogate Rac1-induced stimulation of DNA synthesis and superoxide production. The inconsistencies in the two reports could be attributed to either cell line differences used in the two studies (NIH3T3 vs COS cells), the nature of the transforming mutants used (Rac1 Q61L vs Rac1 G12V), or the method of Rac1 expression (transient vs stable).

The loss of membrane ruffling and actin reorganization observed for the Rac1 deletion mutant in our studies raises the question of whether deletion of the Rac1 insert has introduced a conformational change in the protein, altered the kinetics of nucleotide binding, or affected protein−protein or protein−lipid interactions that may be crucial for downstream signaling. The insert deletion mutant has been widely used as a reagent for functional studies in RhoA, Cdc42, and Rac1, yet its structural and biochemical properties remain uncharacterized. In the studies reported herein, we have characterized the effect of deleting the insert region of Rac1 on its overall structure, thermodynamic stability, kinetics of nucleotide association both in the presence and absence of the exchange factor Vav2, GDI association, and phospholipid interactions. These studies provide quantitative information regarding Rac1−nucleotide, Rac1−GDI, and Rac1−lipid interactions in vitro and provide a structural basis for the observed cellular effects. On the basis of the in vitro studies reported herein, we propose that the loss of membrane ruffling observed for this mutant in vivo is most likely attributed to the attenuation of a key effector interaction that is important for the regulation of the cytoskeleton.

MATERIALS AND METHODS

Protein Expression and Purification. The Rac1·Δ^{ins} mutant (residues 1−188 of Rac1, with deletion of residues 124−134 and introduction of the point mutations P136A and C178S) was subcloned from the mammalian vector pCGN into the Nde I and EcoRI restriction sites of pET21a (Novagen). Unlabeled and uniformly ^{15}N-labeled Rac1·Δ^{ins} was expressed and purified in a manner similar to the wild-type protein using cation-exchange chromatography over an S-sepharose column (Amersham Pharmacia Biotech), followed by gel filtration chromatography using an S100 column (Amersham Pharmacia Biotech). The proteins were >95% pure as judged by SDS PAGE. The identity of the Rac1·Δ^{ins} mutant was confirmed by DNA sequencing as well as by electrospray mass spectrometry. The DH-PH-CRD tridomain of Vav2 was expressed from a pET28a vector (Novagen) and purified using Ni^{2+} affinity chromatography as previously described (*16*). Rho-GDI (gift from G. Bokoch, Scripps Research Institute) was expressed as a GST fusion protein and purified on GSH-agarose beads (SIGMA). Rho-GDI was cleaved off the beads in the presence of thrombin and further purified on an S100 column.

NMR Spectroscopy. Rac1 NMR samples contained 0.5−0.7 mM Rac1 in NMR buffer (20 mM Tris maleate, 50 mM NaCl, 100 μM GDP, 20 mM $MgCl_2$, 10 mM DTT, 0.1% sodium azide) at pH 6.5 in H_2O/ ^2H_2O (90:10). NMR spectra for Rac1 (C178S, 1−188) were collected at 25 °C on Varian Inova 600 or 800 MHz spectrometers equipped with a 5 mm triax or 8 mm *z*-gradient triple resonance probe. All data were collected with a ^{1}H sweep width of 8210 Hz and an ^{15}N sweep width of 2189 Hz, with 512 complex points sampled in the direct dimension, and were acquired in a States-TPPI manner (*17*). Data were processed using the software Felix 98.2 (Accelrys). Resonance assignments for wild-type (WT) Rac1 were obtained using standard triple resonance techniques. Complete assignments and structural characterization of WT Rac1 (residues 1−188, C178S) by solution NMR are the focus of another study (*18*) and will be described elsewhere. Due to limited chemical shift perturbations observed in (^{1}H,^{15}N) HSQC spectra, the Rac1·Δ^{ins} mutant was assigned in a straightforward manner, in comparison to WT Rac1, and the assignments were confirmed from ^{15}N-edited NOESY data. Analysis of NOESY data was performed for WT and the Rac1·Δ^{ins} mutant from data collected at high field (800 MHz). Identical gradient sensitivity enhanced versions (ProteinPack, Varian Inc.) of 75 ms ^{15}N-edited 3D NOESY-HSQC (*19*, *20*) spectra were collected for both WT Rac1 and Rac1·Δ^{ins}. Amide H−D exchange rates were obtained by rapidly diluting a highly concentrated sample of Rac1 (50 μL of Rac1 in 90% ^2H_2O buffer into 700 μL of 99% ^2H_2O NMR buffer) followed by acquisition of (^{1}H,^{15}N) HSQC spectra (dead time = 2 min, acq time = 20 min). Peak intensities were fit to a single exponential using the program Kaleidagraph 3.0.5 (Abelbeck software). ^{31}P spectra were recorded on an Inova 600 MHz spectrometer operating at 243 MHz. One-dimensional ^{31}P spectra were collected with 4000 scans, a spectral width of 60 ppm, and a 65° pulse using a repetition time of 3 s. ^{31}P spectra were referenced to 85% phosphoric acid. Chemical shift mapping studies to test for Rac1−phospholipid interactions were performed by slowly titrating increasing amounts (up to a 5-fold molar excess of phospholipid relative to the amount of Rac1) of either soluble C_4-inositol 4,5-bisphosphate or C_4-inositol 3,4,5-triphosphate (Echelon Inc) into a 0.25 mM solution of Rac1-GDP/Mg^{2+} and by following spectral changes using (^{1}H,^{15}N) HSQC spectra.

Fluorescence Measurements. The dissociation rate constants for intrinsic and GEF (Vav2 DH-PH-CRD)-mediated exchange for WT Rac1 and Rac1·Δ^{ins} were measured by monitoring the decrease in fluorescence intensity due to dissociation of preloaded fluorescent (mant-GDP) nucleotide in the presence of a 400-fold excess of unlabeled nucleotide. Fluorescence measurements were made in 20 mM Tris pH 7.5, 50 mM sodium chloride, 5 mM $MgCl_2$, and 1 mM DTT in a PerkinElmer LS 50B fluorescence spectrometer, with excitation and emission wavelengths of 358 and 440 nm,

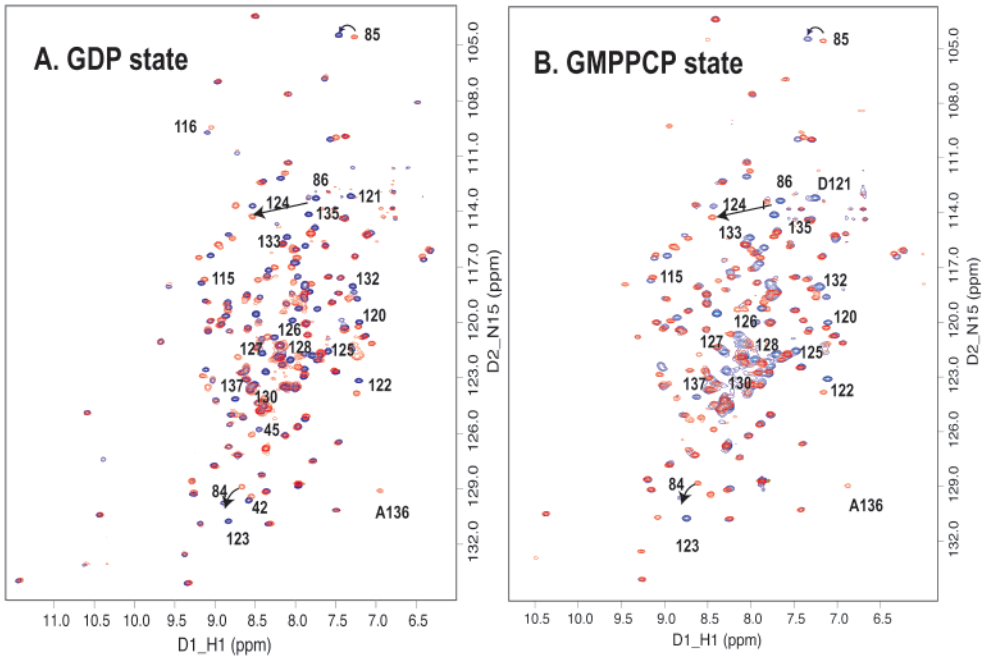

FIGURE 1: Overlay of (^{1}H,^{15}N) HSQC spectra of uniformly ^{15}N-labeled Rac1 WT (in blue) and Rac1·Δ^{ins} (in red) in (A) GDP·Mg^{2+} and (B) GMPPCP·Mg^{2+} bound forms. Spectra were obtained at pH 6.5 and 25 °C. Insert residues that are absent in the deletion mutant and residues with the largest chemical shift changes are labeled.

respectively, and monitored for 2 h at 37 °C for the intrinsic rates and at 25 °C for the Vav2-mediated rates. The rates of nucleotide dissociation were also obtained under multiple turnover conditions (i.e., by increasing the concentration of Rac1·3′mantGDP[1] at a constant concentration of Vav2 DH-PH-CRD. The fluorescence intensity at the end point was obtained by adding 50 mM EDTA (final concentration) to the cuvette. Fluorescence titrations for the interactions of WT Rac1 and Rac1·Δ^{ins} with Rho-GDI were carried out by adding increasing amounts of Rho-GDI to 3 mL of Rac1·3′mantGDP in the above buffer and monitoring the increase in fluorescence anisotropy with each addition. The excitation and emission wavelengths were 358 and 440 nm, respectively. Equilibrium dissociation constants were obtained by plotting the change in fluorescence anisotropy as a function of [GDI] added and fitting the data to a hyperbolic function assuming a single binding site for the interaction using the program Kaleidagraph 3.0.5. Inhibition of mant-GDP dissociation from Rac1 in the presence of a 10-fold excess of GDI was performed as described above at 25 °C.

Chemical Denaturation Studies. Rac1 and the deletion mutant were dialyzed extensively against 10 mM sodium phosphate pH 7.0, 0.1 M sodium chloride, 5 mM $MgCl_2$, 0.1 mM GDP, and 1 mM DTT. The protein was diluted to varying final urea concentrations in the above buffer and equilibrated for 48 h at 25 °C prior to data collection. Final Rac1 concentrations ranged from 10 to 16 μM. The equilibrium unfolding reaction was monitored using chemical (urea) denaturation by following the change in circular dichroism at 222 nm using a path length of 1 cm. Equilibrium unfolding data for ternary Rac1·GDP·Mg^{2+} and Rac1·GMPPCP·Mg^{2+} were fit to a two-state model, as previously described (*21*):

$$N \overset{K}{\rightleftharpoons} U + Mg^{2+} + GDP$$

N is the native state, U the unfolded state without ligands, and GDP and Mg^{2+} are the free ligands. The program Kaleidagraph 3.0.5 was used to fit the data.

Phospholipid Overlay Assays. To test for phospholipid binding, phospholipid PIP-Strips (Echelon Inc.) with twelve phospholipids (at 100 pmol/spot) were blocked with 3% (w/v) fatty acid-free BSA in TBST buffer (10 mM Tris pH 8.0, 150 mM NaCl, 0.1% Tween-20) for 2 h at room temperature. The blots were washed three times in TBST buffer and then incubated with 500 ng/mL of either wild type or mutant Rac1 (Δ^{ins} or Rac1(1−177) mutants) in 3% fatty acid-free bovine serum albumin (BSA) in TBST buffer overnight at 4 °C. The blots were washed three times with TBST buffer and then incubated for 2 h at room temperature with a goat polyclonal primary antibody toward the carboxy terminus of Rac1 (Santa Cruz Biotechnology, Inc). This procedure was followed by extensive washing of the blots and incubation with a peroxidase conjugated goat anti-mouse secondary antibody (Pierce). The blots were washed extensively and visualized using enhanced chemiluminescence (ECL).

RESULTS

Overall Structure. The resonance frequencies of individual amide protons in NMR spectra are acutely sensitive to the chemical and electronic environment of the nucleus and reflect structural perturbations due to the introduction of a mutation. Comparison of (^{1}H,^{15}N) HSQC spectra of the insert deletion mutant to that of WT Rac1 (Figure 1) reveals that deletion of 13 amino acids from Rac1 has no effect on the resonance frequencies of most residues in the protein. Chemical shift perturbations observed in either Rac1·Δ^{ins}·GDP·Mg^{2+} or Rac1·Δ^{ins}·GMPPCP·Mg^{2+} are small and limited to the local environment around the site of mutation.

[1] Abbreviations: mantGDP, fluorescent analogue of GDP containing the fluorescent mant group, 2′,3′-(*N*-methylanthraniloyl); GEF, guanine nucleotide exchange factor; GDI, guanine nucleotide dissociation inhibitor; NMR, nuclear magnetic resonance; CD, circular dichroism.

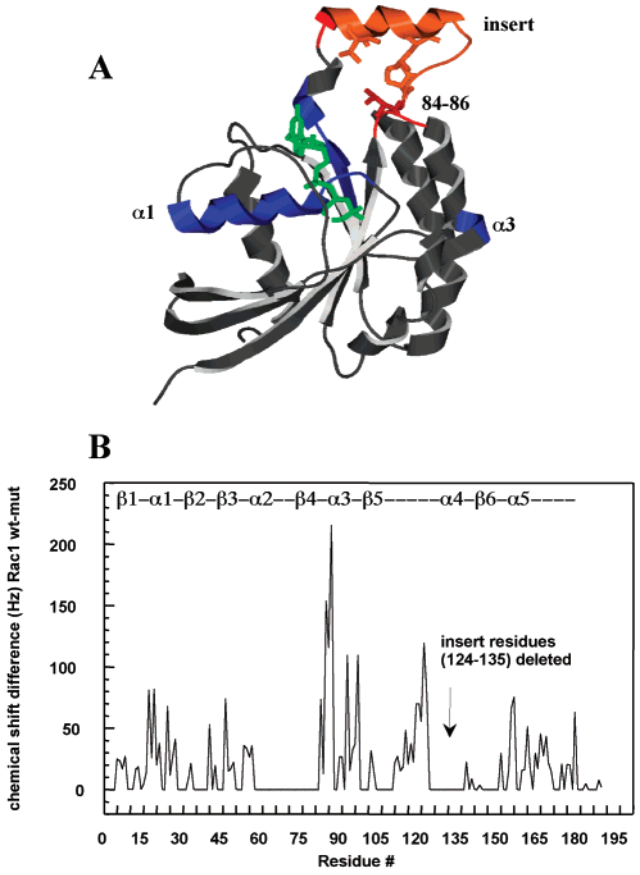

FIGURE 2: (A) Residues that show significant chemical shift perturbations are mapped onto the Rac1·GMPPNP·Mg^{2+} crystal structure (PDB code 1MH1). The largest perturbation is observed for Leu84, Val85, and S86. The side chain of Val85 packs against residues Thr125, Ile126, Leu129, and Pro136 of the insert in the Rac1·GMPPNP·Mg^{2+} crystal structure. The insert region is shown in orange. Residues with shifts greater that 1 line width are shown in red, whereas residues that show shifts ($\leq$1 line width) or are exchange-broadened are depicted in blue. (B) The total magnitude ($^1H + ^{15}N$) of chemical shift perturbations (in Hz) observed in (^1H,^{15}N) HSQC spectra plotted vs residue number for Rac1·GDP·Mg^{2+} The Figure was generated using the program SPOCK (Jon A. Christopher, Department of Biochemistry and Biophysics, Texas A & M University).

As expected, deletion of 12 residues in Rac1 results in the loss of 12 resonances from the spectrum and shows the presence of a new cross-peak for A136 because this residue is a proline in native Rac1.

The largest chemical shift perturbations observed in HSQC spectra of both Rac1·GDP·Mg^{2+} and Rac1·GMPPCP·Mg^{2+} are for residues L84, V85, S86, D122, K123, and I137 (Figures 1 and 2). These residues either flank (residues D122, K123, I137) or lie in close proximity to the insert (residues L84−S86) in the Rac1·GMPPNP·Mg^{2+} crystal structure (*9*). In the Rac1 crystal structure, the side chain of V85 packs against the side chains of residues T125, I126, L129, and P136 of the insert, forming a loosely defined hydrophobic core, although backbone amides in the 84−86 loop are >5 Å away from any other backbone or side-chain atom in the protein. Deletion of the insert residues does not result in NOE changes for loop residues 84−86 in 3D ^{15}N-edited NOESY spectra of Rac1·Δ^{ins}. In addition, a residue-by-residue comparison of NOESY cross-peaks in 3D ^{15}N-edited NOESY spectra of the Rac1·Δ^{ins} mutant reveals no major differences between WT and the Rac1·Δ^{ins} mutant, even for those cross-peaks that are shifted in the HSQC spectra. Intriguingly, loop residues L84, V85, and S86 show a paucity of both intra- and interresidue NOEs in both the wild type and the mutant, suggesting that either these backbone amides or side chains (due to conformational averaging of their side chains) do not adopt a well-defined or fixed conformation in solution or the backbone amides of residues 84−86 show a high degree of internal motion. Nevertheless, the chemical shift perturbations and NOE data taken together indicate that deletion of the insert does not result in a major conformational change in either Rac1·GDP·Mg^{2+} or Rac1·GMPPCP·Mg^{2+}.

These NMR data are also substantiated by the amide proton hydrogen exchange rates of the Rac1·Δ^{ins} mutant. The protection of amide protons from exchange with solvent water is influenced by the primary, secondary, and tertiary structure of a polypeptide. Amide protons that are buried (and hence inaccessible to solvent) or those that are in well-defined secondary structure elements (and hence hydrogen bonded) exchange slowly ($k_{ex} < 10^{-2}$ s^{-1}) with bulk water in solution. Comparison of H−D exchange rates between wild-type and mutant proteins reveals no major differences in the exchange behavior for most amide protons. Only five residues show significant differences in their amide proton exchange rates in the Rac1·Δ^{ins} mutant relative to that in WT Rac1. Residues R120 and S86 show increases in their exchange rates by 1000-fold and 100-fold, respectively (Figure 3). The observed increase is not surprising: R120 lies in a helical turn just preceding the insert, and deletion of the insert region forces it into a loop, thus rendering it more solvent-accessible. Similarly, S86 is more solvent-exposed in the mutant because of the loss of the hydrophobic interaction of insert residues T125, I126, and L129 with V85. In addition, three residues that lie in the nucleotide-binding pocket (K116, G114, C18) show decreased amide exchange rates in the mutant protein relative to that in the wild type, which is consistent with a slight decrease in the dissociation rate of the mutant (see below) and may reflect a small stabilization of the nucleotide-binding pocket upon insert deletion. Residues 122, 123, and 137 exchange too rapidly after H−D exchange in both the wild-type and mutant proteins to be detected in the first HSQC spectrum; hence, any difference in their exchange rates cannot be measured by the H−D method. The amide proton of V85 remains well-protected in both WT Rac1 and Rac1·Δ^{ins}, and no difference in its exchange rate is observed. The chemical shift data, NOEs, and amide exchange rates suggest that even though residues 84−86 lie in proximity to the insert region deletion of insert residues 124−134 does not result in a major conformational change in the β4/α3 loop in the protein.

In addition to perturbations observed for loop residues 84−86 and residues flanking the insert, small perturbations (of ~1 line width) or decreased intensities are also observed for residues that lie near the nucleotide-binding pocket (i.e., in the phosphate-binding loop (residues 13−18) or the guanine-recognition loops (residues 113−118)). In addition, small chemical shift perturbations are observed for residues 19−25 of α-helix 1 and 94−95 of α-helix 3. However, our findings that no NOE and H−D differences are observed for most residues reflect minor changes in the local environment of these nuclei in response to mutation.

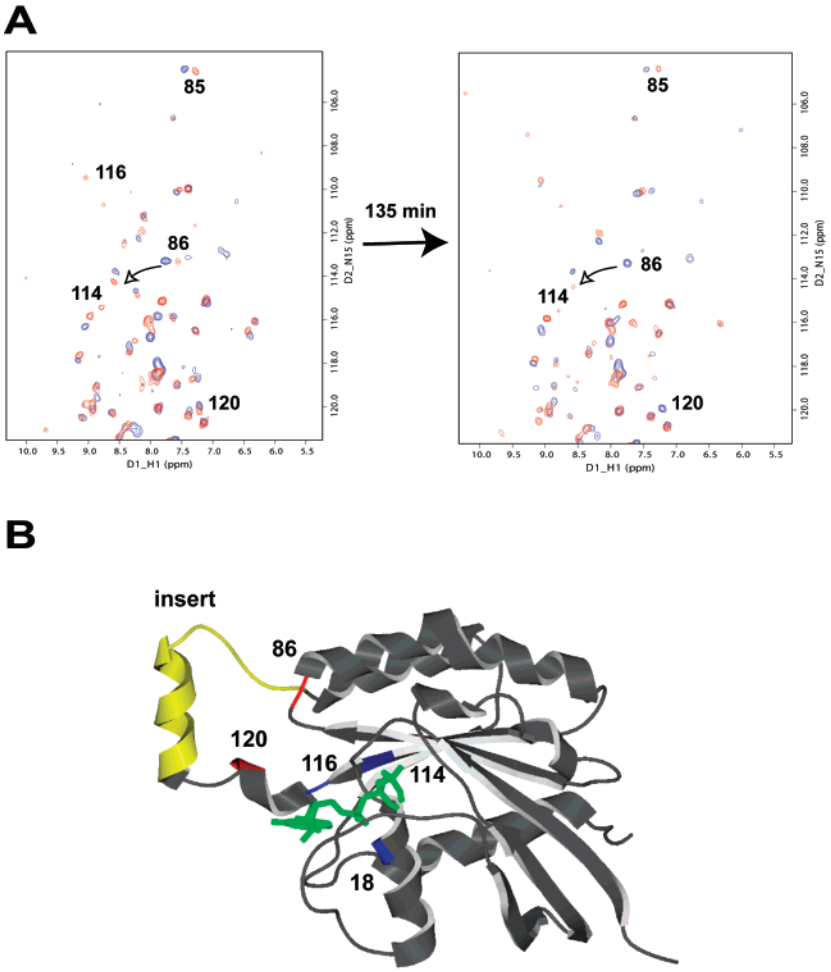

FIGURE 3: Protection of amide protons from H−D exchange in Rac1·Δ^{ins}·GDP·Mg^{2+} (red) compared to that of Rac1·GDP·Mg^{2+} (blue). The spectrum on the left was initiated 2 min after the addition of ^2H_2O, whereas the one on the right was taken after >2 h (135 min). Residues that show a significant difference between wild-type and mutant proteins are labeled. (B) Residues that show significant differences in amide exchange behavior are mapped onto the crystal structure of Rac1·GMPPNP. The insert region is depicted in yellow, R120 and S86, in red, and G114, K116, and C18, in cyan.

Global Stability. The NMR studies performed on the deletion mutant indicate that there are no structural changes in Rac1 upon deletion of the insert. However, does deletion of the insert affect the conformational stability of Rac1, and are there any functional consequences associated with it? To understand how the insert region alters the energetics of Rac1 structure, we compared the global stability of the wild-type and mutant proteins. It has previously been shown that solvent (urea) denaturation can be used to assess the global stability of H-Ras (*21*). Similar H-Ras, we found that Rac1 underwent a reversible unfolding−refolding transition and that the equilibrium behavior fit well to a simple two-state model (see Methods and Materials). As shown in Figure 4 and Table 1, deletion of the insert causes a small (average = 0.87 kcal/mol; range = 0.72−1.0 kcal/mol depending upon the *m* value used) decrease in the global stability of Rac1·GDP·Mg^{2+} and no change in the stability of the active GMPPCP-bound form. The midpoint of the unfolding transition (C_{mid}) for the mutant decreases by 0.4 M urea in the GDP-bound form but remains unchanged in the active GMPPCP form. The small decrease in stability of the insert mutant by less than 1 kcal/mol in the inactive Rac1·GDP·Mg^{2+} form may be due to the loss of side chain−side chain interactions between insert residues with V85. Alternatively, they may reflect the decreased stability of the native state or the increased stability of the unfolded state of the mutant relative to that of the wild type. Nevertheless, the chemical denaturation data are consistent with NMR studies showing no major structural perturbations due to insert deletion. Intriguingly, the GMPPCP-bound form of wild-type Rac1 is ~2.0 kcal/mol less stable than the wild-type GDP form. NMR characterization of the structural and dynamic properties of the GDP- and GMPPCP-bound forms of Rac1 (*18*) should help identify the source of this destabilization.

GDP Dissociation. Although the insert region does not make direct contact with the bound nucleotide in any of the known structures, residues at the end of β-strand-5 and the beginning of loop 8 (116−120) in all GTPases interact with the N7 atom of the guanine ring and flank the insert region. Since our NMR data indicated that small chemical shift perturbations were observed for residues in the phosphate and guanine nucleotide-binding loops, we determined the GDP dissociation rates both in the presence and absence of the guanine nucleotide-exchange factor Vav2. Previous studies (*16*) have shown that the DH−PH−CRD tridomain of Vav2 is the minimal fragment required for guanine nucleotide-exchange activity and signaling in vivo; hence, Vav2 DH−PH−CRD was used in our studies to assess the contribution of the insert region to the rate of nucleotide dissociation (Figure 5). We found that deletion of the insert

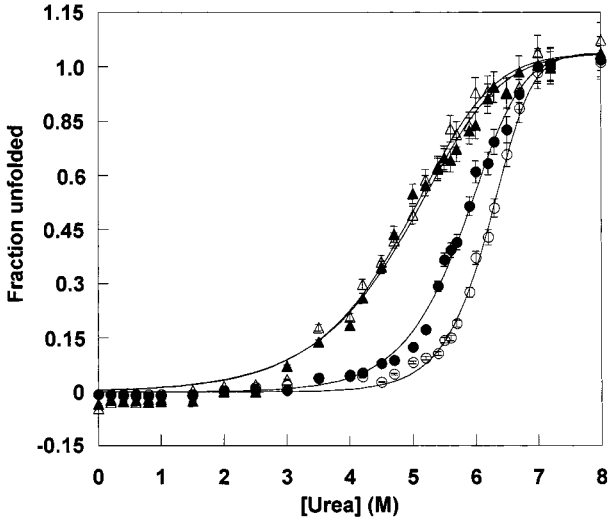

FIGURE 4: Representative urea denaturation curves for Rac1·GDP·Mg^{2+} (▲), Rac1·Δ^{ins}·GDP·Mg^{2+} (△), Rac1·GMPPCP·Mg^{2+} (●), and Rac1·Δ^{ins}·GMPPCP·Mg^{2+} (○). Unfolding transitions were monitored using circular dichroism at 222 nm, and the data were fit to a two-state unfolding model as described in the text. C_{mid} and *m* values were obtained from an average of two experiments and are reported in Table 1.

Table 1: Analysis of Urea Denaturation Curves at pH 7.0 and 25 °C

protein	c_{mid} (M urea)	*m* (kcal mol^{-1} M^{-1})
Rac1·GDP·Mg^{2+}	6.12 ± 0.01	2.39 ± 0.078
Rac1·Δ^{ins}·GDP·Mg^{2+}	5.7 ± 0.03	1.78 ± 0.065
Rac1·GMPPCP·Mg^{2+}	4.8 ± 0.05	1.17 ± 0.068
Rac1·Δ^{ins}·GMPPCP·Mg^{2+}	4.8 ± 0.01	1.14 ± 0.062

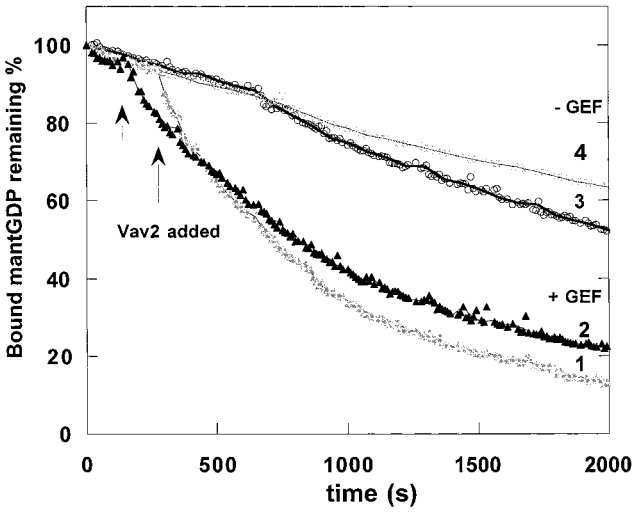

FIGURE 5: Measurement of the intrinsic (3,4) and GEF- (Vav2 DH−PH−CRD) mediated (1,2) GDP release rates for Rac1·GDP·Mg^{2+} (○, ▲; black) and Rac1·Δ^{ins}·GDP·Mg^{2+}(○, ▲; gray). The Rac1 proteins were preloaded with mantGDP, and the decay of fluorescence intensity in the absence of GEF was monitored in the presence of a 1000-fold excess of unlabeled GDP for 2 h at 37 °C. The GEF-facilitated GDP dissociation rates were measured at Rac1/GEF ratios of 1:10 to 1:100 in the presence of a 400-fold excess of GDP at 25 °C. The fluorescence decay curves depicted are for a Rac1/Vav2 ratio of 1:100.

causes a small (1.5-fold) *decrease* in the intrinsic rate of exchange and a 3-fold *increase* in the GEF (Vav2 DH−PH−CRD) stimulated exchange rate. The increase in the GEF stimulated rate is intriguing and was observed under multiple

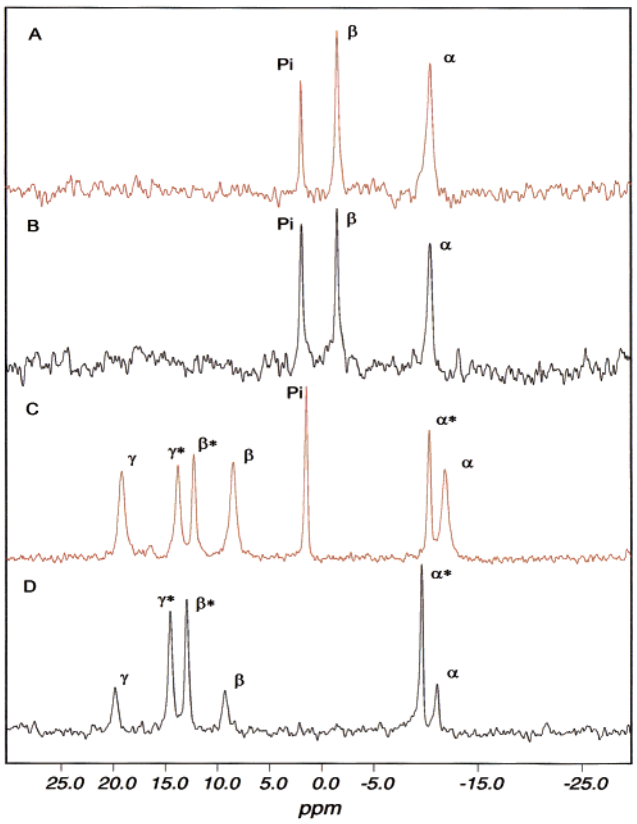

FIGURE 6: ^{31}P NMR spectra of (A) wild-type Rac1·GDP·Mg^{2+}, (B) Rac1·Δ^{ins}·GDP·Mg^{2+}, (C) wild-type Rac1·GMPPCP·Mg^{2+}, and (D) Rac1·Δ^{ins}·GMPPCP·Mg^{2+} collected on an Inova 600 MHz spectrometer at 25 °C and pH 6.8. Two sets of resonances are observed for the GMPPCP form. Resonances labeled with an asterisk (∗) correspond to free GMPPCP in solution, and the second set corresponds to the Rac1 bound form of GMPPCP. ^{31}P spectra were also collected at 5 and 15 °C, and no change in either the wild-type or mutant spectra were observed.

turnover conditions as well (data not shown). Because the insert is not directly involved in the binding interface between GEFs and GTPases (*22*), it is possible that deletion of the insert affects a rate-limiting step in GDP dissociation. It is also plausible that the decreased dissociation rate reflects small changes in backbone or side chain dynamics for residues in the phosphate binding loop or the guanine recognition loops. The effect of insert deletion on backbone dynamics will be described elsewhere (*18*). Nevertheless, the observed effect on the kinetics of GDP dissociation is small, especially when compared to those observed for transforming Ras mutants (for example, F28L H-Ras shows a 140-fold increase in the rate of GDP dissociation compared to that of H-Ras wild type (*23*)) and are unlikely to contribute to the observed biological effects of the mutant in vivo. A change in the environment of the bound nucleotide would also be reflected in the chemical shifts of the ^{31}P NMR spectra of the insert mutant. The chemical shifts of the α-, *β*-, and *γ*- phosphate resonances of the bound nucleotide are the same in the insert and the wild-type protein (Figure 6), indicating that the environment for GDP in the Rac1 deletion mutant is similar to that in the wild-type protein.

Rac1−GDI Interactions. Rho proteins exist in the cytosol in their inactive GDP bound forms in complex with Rho guanine nucleotide dissociation inhibitor or Rho-GDI (for a

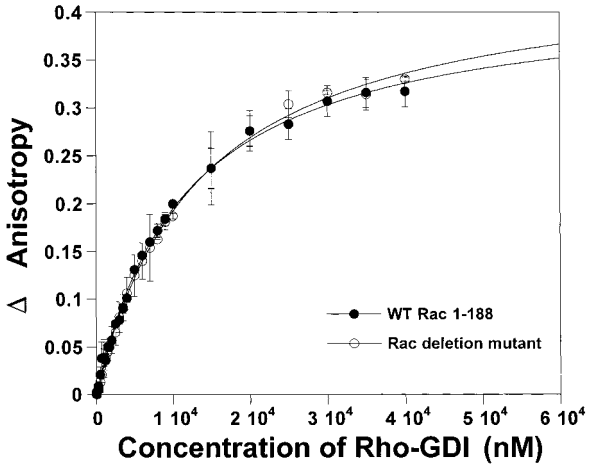

FIGURE 7: Association of non-prenylated Rac1·GDP·Mg^{2+} (▲), Rac1·Δ^{ins}·GDP·Mg^{2+} (△), with Rho-GDI, measured using fluorescence anisotropy. The change in fluorescence anisotropy is plotted against GDI added, and the resulting data were fit to a hyperbolic equation to obtain dissociation constants.

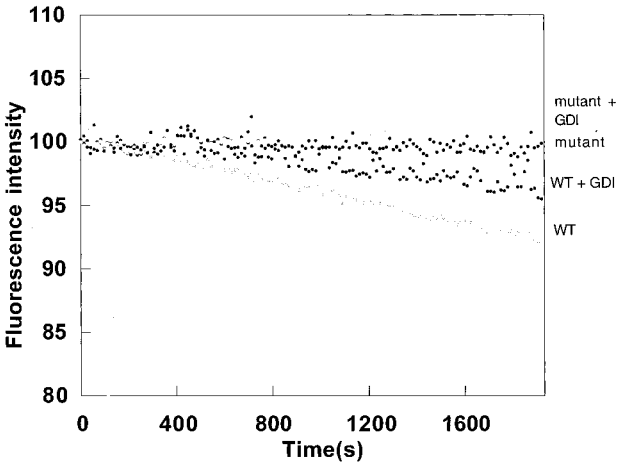

FIGURE 8: Comparison of GDI-induced inhibition of GDP dissociation for non-prenylated Rac1·GDP·Mg^{2+} (without GDI (1), with GDI (2)) and Rac1·Δ^{ins}·GDP·Mg^{2+} (without GDI(3), with GDI(4)). The release of mantGDP from preloaded Rac1·mantGDP·Mg^{2+} was followed using fluorescence at 37 °C and pH 7.5 and in the presence of increasing concentrations of GDI. The fluorescence decay curves depicted are for a Rac1/GDI ratio of 1:10.

review see *24*). Upon activation, Rho proteins dissociate from GDI and are translocated to the plasma membrane. Previous studies on Cdc42 have shown that the insert region does not affect the affinity of Cdc42 for Rho-GDI (*25*). Intriguingly, however, the Cdc42 insert deletion mutant was found to be less susceptible to GDI-mediated inhibition of GDP dissociation. To ascertain the effect of insert mutation on Rac1−GDI interactions, we first compared the association of nonprenylated Rac1·GDP·Mg^{2+} and Rac1·Δ^{ins} ·GDP·Mg^{2+} toward Rho-GDI. The studies were performed in the absence of the prenyl moiety so as to pick up small differences in binding in response to insert deletion. The results show that as is predicted from the crystal structures (*26, 27*) deletion of the insert region has no effect on GDI interactions (Figure 7). The K_D for the interaction of nonprenylated WT Rac1 toward Rho-GDI was found to be 11.8 ± 0.4 μM and that of nonprenylated Rac1·Δ^{ins}−GDI, 14.3 ± 0.7 μM. Hence, the K_D's for the interaction of WT and Rac1·Δ^{ins} are similar. These data are consistent with previous studies that show that although the prenyl group may increase the affinity of GDI for Rac1 it is not necessary for the association of Rac1 with GDI (*28*−*30*).

In addition to the association of Rac1 with GDI, we also compared GDI-mediated inhibition of GDP release from Rac1 (Figure 8). The results show that in the presence of a 10-fold excess of Rho-GDI WT Rac1 exhibits a 2-fold decrease in the rate of GDP dissociation whereas the insert deletion mutant shows no inhibition of GDP release in the presence of GDI. However, because the intrinsic rate of mantGDP dissociation is slow (2-fold lower in the deletion mutant), a further decrease in response to GDI is probably not observed during the time scale of the experiment. The apparent "lack of inhibition" of GDP dissociation observed for the RacΔ^{ins} mutant is hence due to the intrinsically lower dissociation rate of the mutant and has no bearing on its association with Rho-GDI.

Rac1−*Phospholipid Interactions.* Previous studies using pull-down assays have reported that the insert and the C-terminus are important for the interaction of Rac1 with the anionic phospholipids PtdIns(3,4,5)P_3 and PtdIns(3,4)P_2 (*31*). Because these in vitro studies were performed with a mutant that lacked both the insert region and 33 amino acids from the C-terminus of the protein, we decided to further investigate Rac1−phospholipid interactions. Karnoub et al. (*6*) have shown that the insert deletion mutant does not affect cellular localization of Rac1 in vivo. We therefore characterized the interactions of the wild type and mutant proteins (Rac1·Δ^{ins} and Rac1−177, which lacks the basic region) with phospholipids using solution NMR and phospholipid overlay assays (see Methods). The NMR studies were performed by titrating a 5-fold excess of the soluble C_4-inositol 4,5-bisphosphate (C_4-PIP_2) and C_4-inositol 3,4,5-triphosphate (C_4-PIP_3) into a 0.25 mM solution of ^{15}N-labeled WT Rac1 and monitoring chemical shift perturbations in (^{1}H,^{15}N) HSQC spectra. Chemical shifts in NMR spectra are extremely sensitive to macromolecular interactions; however, contrary to previously reported studies (*31*), titration of soluble C_4−PIP_2 or C_4−PIP_3 analogues into the WT Rac1 NMR sample did not induce any spectral perturbations in the Rac1 (^{1}H,^{15}N) HSQC spectrum, and the spectra with and without (a 10-fold molar excess of) phospholipids were indistinguishable (data not shown). Because it is possible that the interaction of Rac1 with phospholipids requires a membrane bilayer, we also tested the interactions of wild-type and mutant Rac1 proteins using a phospholipid overlay assay in which liposomes containing different phospholipid analogues were spotted onto nitrocellulose membranes. The assay was repeated three times using a Rac1 concentration range of 1 μg/mL to 0.1 mg/mL, but no interaction with either the wild-type or mutant proteins was detected. Therefore, the data indicate that in the absence of a geranylgeranyl moiety the interaction of Rac1 with phospholipids is weak at best and the prenyl moiety must be the main driving force for membrane association.

DISCUSSION

The insert deletion mutant has been used widely as a reagent for cell biological studies, yet there seems to be considerable disparity in the literature as to the functional consequence of deleting this region in RhoA, Rac1, or Cdc42.

Studies on a Rac−Rho chimera (*32*), wherein insert residues 122−135 of RhoA were replaced with those of Ras, have shown that the mutant protein retains effector binding toward PRK2 and ROCK-1 but decreases transformation of NIH3T3 cells and abolishes stress fiber formation. Recent studies suggest that these effects on transformation and the actin cytoskeleton might be mediated via Rho kinase (*33*, *34*) because the RhoA insert deletion mutant is capable of interacting with Rho kinase but it does not activate it. In Cdc42, deletion of the insert region abolishes its ability to transform NIH3T3 cells (*14*) but has no effect on either the actin cytoskeleton or JNK1 activation (*14*). Substitution of loop 8 of Ras for the insert region of Cdc42 results in a chimeric protein that shows wild-type exchange activity toward the GEF Dbl as well as wild-type GAP-mediated GTP hydrolysis but is no longer susceptible to GDI-induced inhibition of GDP dissociation. The insert region of Cdc42 is also reported to be important for association with the Cdc42 effectors IQGAP1 and IQGAP2 (*35*), whereas it modulates the activity of phospholipase D1 (*33*) but does not affect association with it. In Rac1, the closest homologue of Cdc42, functional studies show no effect of insert deletion on transformation, NF-κB activation, or ROS production in vivo. However, we have shown that in contrast to Joneson and Bar-Sagi (*15)* deletion of the insert has a dramatic effect on SRF activation and regulation of the actin cytoskeleton such that cells expressing the insert deletion mutant are no longer capable of lamellipodia formation (*6*).

These functional studies performed so far yield a number of testable hypotheses as to the effect of deleting the insert region in Rac1. First, deletion of the insert region could result in a conformational change in Rac1, thereby preventing association with downstream effectors that are necessary for the observed cellular effects. Second, it could alter the kinetics of nucleotide dissociation, thus altering the population of "active" GTP-bound Rac1 in vivo. Third, the insert region may mediate interactions with specific effectors that are important for activating signal transduction pathways. Finally, there are contradictory reports that suggest that insert deletion could alter membrane localization and thus decrease the available pool of Rac1 for cell signaling. To address each of these possibilities outside the context of the cellular milieu, we have characterized the structural, biophysical, and biochemical properties of the Rac1 insert deletion mutant. Results from our NMR studies show that small chemical shift perturbations are observed upon insert deletion in Rac1·GDP·Mg^{2+} or Rac1·GMPPCP·Mg^{2+}. Residues in close proximity to the insert (i.e., residues D122, K123, I137, L84-S86) show the greatest perturbations in NMR spectra. In addition, residues in α-helix 1 (residues 19−25) and α-helix 3 (residues 94−95) show small but significant chemical shift perturbations. These chemical shift changes most likely reflect subtle changes in the chemical environment because comparison of NOE intensities or amide exchange rates shows no change in these NMR parameters between wild-type and mutant forms, consistent with the lack of large chemical shift perturbations. ^{31}P NMR analysis also shows no change in the chemical shifts of the α-, β-, or γ- phosphate resonances of the bound nucleotide in either the GDP- or GMPPCP-bound forms. Therefore, deletion of 12 residues maintains the environment of the nucleotide-binding pocket and the overall α/β topology of Rac1, which is necessary for binding the nucleotide. The NMR studies are further supported by chemical denaturation studies that show that the insert mutant is not significantly destabilized relative to the stability of the wild type. Hence, the functional consequences of Rac1 deletion cannot be attributed to either a conformational change in the protein or decreased stability of the mutant in vivo.

To assess whether the cellular effects may be due to a change in the kinetics of nucleotide binding of Rac1 for the bound nucleotide and hence a change in GTP/GDP cycling, we compared the intrinsic and GEF-mediated GDP dissociation rates for wild-type and mutant Rac1. The data show a (small) 1.5-fold decrease in the intrinsic rate of dissociation and a 3-fold increase in the GEF-mediated exchange rate of the Rac1·Δ^{ins} mutant versus that of WT Rac1. Because the NMR data do not suggest a large-scale structural change for residues that are important for nucleotide association, the small acceleration in the GEF-mediated dissociation rate most likely reflects subtle changes in the nucleotide-binding pocket that contribute to the exchange mechanism. These effects are small when compared to the effects of the transforming mutations F28L (*23*) and N17A (*36*) that either increase the rate of nucleotide cycling or populate Rac1 in the apo form, respectively.

We have also looked into the possibility that deletion of the Rac1 insert affects association with phospholipids. These studies were done in vitro, first by examining spectral perturbations introduced in WT Rac1 NMR spectra as a function of added soluble phospholipid and second by monitoring the binding of wild-type and mutant Rac1 proteins in a dot blot assay wherein liposomes containing phospholipids were spotted onto nitrocellulose, thereby increasing the local concentration of phospholipids available for the interaction. NMR studies are very sensitive to changes in the electronic environments of nuclei; however, we were unable to see any association of Rac1 with phospholipids. The lack of association observed in our studies suggests strongly that unlike PH, FYVE, or PX domains that bind phospholipids with high affinity (*37*) the interaction of nonprenylated Rac1 with phospholipids is at best very weak. The main driving force for membrane interaction is the geranylgeranyl moiety. These in vitro results reinforce our earlier in vivo observations that the Rac1 insert deletion mutant does not mislocalize relative to native Rac1 (*6*).

Finally, deletion of the insert does not impair the association of Rac1 with GDI. Our fluorescence measurements suggest that there is no change in the equilibrium dissociation constant for the Rac1−GDI interaction. No significant impairment in GDI-mediated inhibition of GDP dissociation is observed for the Rac1·Δ^{ins} mutant, which is most likely due to the 2-fold decrease in the intrinsic dissociation rate of Rac1·Δ^{ins}·GDP·Mg^{2+} compared to that of WT Rac1·GDP·Mg^{2+}.

Hence, our characterization of the structural, biochemical, and biophysical properties of Rac1·Δ^{ins}·GDP·Mg^{2+} suggests that this molecule retains all of its intrinsic GTPase properties, is perfectly capable of cycling guanine nucleotides, can interact with GDI, and can be activated by exchange factors. We suggest that the inability of this mutant to trigger lamellipodia formation in NIH3T3 cells is therefore most likely due to the loss or alteration of a key effector interaction that is necessary for SRF activation and regulation of the

actin cytoskeleton. There are numerous reports in the literature that implicate the insert region of Rho proteins as being necessary for downstream effector activation or interaction. The insert region of Rac1 is deemed important for direct interaction with at least one component of the NADPH oxidase complex, possibly cytochrome b_{558}, because deletion of the insert region is reported to inhibit oxidase activation (*13*). Using pull-down assays, others (*35*) have shown that the insert region of Cdc42 is important for its association with IQGAP1 and IQGAP2 (). Hence, it is very likely that similar to the two switch regions of the GTPases the solvent-exposed, charged surface of the insert forms either a distinct binding site or a secondary binding site for an effector molecule that is specific for actin regulation. Structural studies on Rho-CRIB motifs (*38*, *39*) reveal that Rho proteins use regions other than the two switch regions, such as the extreme C-terminus, to bind to CRIB-containing targets. Therefore, it is likely that the insert region is also important either for direct effector recognition or for inducing conformational changes necessary for the activation of targets. A likely candidate that is known to be involved in lamellipodia formation is PI3K (*40*). Future studies will test this hypothesis.

REFERENCES

1. Khosravi-Far, R., Campbell, S., Rossman, K. L., and Der, C. J. (1998) *Adv. Cancer Res.* 57−107.
2. Zohn, I. M., Campbell, S. L., Khosravi-Far, R., Rossman, K. L., Der, C. J. (1998) *Oncogene 17*, 1415−1438.
3. Narumiya, S. (1996) *J. Biochem. (Tokyo) 120*, 215−228.
4. Symons, M. (1996) *Trends Biochem. Sci. 21*, 178−181.
5. Hall, A. (1998) *Science 279*, 509−514.
6. Karnoub, A. E., Der, C. J., and Campbell, S. L. (2001) *Mol. Cell. Biol. 21*, 2847−2857.
7. Kraulis, P. J., Domaille, P. J., Campbell-Burk, S. L., Van Aken, T., and Laue, E. D. (1994) *Biochemistry 33*, 3515−3531.
8. Pai, E. F., Kabsch, W., Krengel, U., Holmes, K. C., John, J., and Wittinghofer, A. (1989) *Nature 341*, 209−214.
9. Hirshberg, M., Stockley, R. W., Dodson, G., and Webb, M. R. (1997) *Nat. Struct. Biol. 4*, 147−152.
10. Feltham, J. L., Dotsch, D., Raza, S., Manor, D., Cerione, R. A., Sutcliffe, M. J., Wagner, G., and Oswald, R. E. (1997) *Biochemistry 36*, 8755−8766.
11. Wei, Y., Zhang, Y., Derewenda, U., Liu, X., Minor, W., Nakamoto, R. K., Somlyo, A. V., Somlyo, A. P., and Derewenda, Z. S. (1997) *Nat. Struct. Biol. 4*, 699−703.
12. Ihara, K., Muraguchi, S., Kato, M., Shimizu, T., Shirakawa, M., Kuroda, S., Kaibuchi, K., and Hakoshima, T. (1998) *J. Biol. Chem. 273*, 9656−9666.
13. Nisimoto, Y., Freeman, J. L., Motalebi, S. A., Hirshberg, M., Lambeth, J. D. (1997) *J. Biol. Chem. 272*, 18834−18841.
14. Wu, W. J., Leonard, D. A., Cerione, R. A., and Manor, D. (1998) *J. Biol. Chem. 273*, 16655−16658.
15. Joneson, T., and Bar-Sagi, D. (1998) *J. Biol. Chem. 273*, 17991−17994.
16. Abe, K., Rossman, K. L., Liu, B., Ritola, K. D., Chiang, D., Campbell, S. L., Burridge, K., and Der, C. J. (2000) *J. Biol. Chem. 275* (14), 10141−10149.
17. Marion, D., Ikura, M., and Bax, A. (1989) *J. Magn. Reson. 85*, 393−399.
18. Thapar, R., and Campbell, S. Unpublished results.
19. Kay, L. E., Keifer, P. A., and Saarinen, J. (1992) *J. Am. Chem. Soc. 114*, 10663.
20. Zhang, O., Kay, L. E., Olivier, J. P., and Forman-Kay, J. D. (1994) *J. Biomol. NMR 4*, 845.
21. Zhang, J., and Matthews, R. C. (1998) *Biochemistry 37*, 14881−14890.
22. Worthylake, D. K., Rossman, K. L., and Sondek, J. (2000) *Nature 408* (6813), 682−688.
23. Reinstein, J., Schlichting, I., Frech, M., Goody, R. S., and Wittinghofer, A. (1991) *J. Biol. Chem. 266*, 17700−17706.
24. Sasaki, T., Takai, Y. (1998) *Biochem. Biophys. Res. Commun. 245* (3), 641−645.
25. Wu, W. J., Leonard, D. A., Cerione, R., and Manor, D. (1997) *J. Biol. Chem. 272*, 26153−26158.
26. Scheffzek, K., Stephan, I., Jensen, O. N., Illenberger, D., Gierschik, P. (2000) *Nat. Struct. Biol. 7* (2), 122−126.
27. Grizot, S., Fauré, J., Fieschi, F., Vignais, P. V., Dagher, M.-C., and Pebay-Peyroula, E. (2001) *Biochemistry 40*, 10007−10013.
28. Nomanbhoy, T. K., Erickson, J. W., Cerione, R. A. (1999) *Biochemistry 38*, 1744−1750.
29. Lian, Y., Barsukov, I., Golovanov, A. P., Hawkins, D. I., Badii, R., Sze, H.-K., Keep, N. H., Bokoch, G. M., and Roberts, G. C. K. (2000) *Structure 8*, 47−55.
30. Fauré, J., and Dagher, M.-C. (2001) *Biochimie 83*, 409−414.
31. Missy, K., Van Poucke, V., Raynal, P., Viala, C., Mauco, G., Plantavaid, M., Chap, H., and Payrastre, B. (1998) *J. Biol. Chem. 273*, 30279−30286.
32. Zong, H., Raman, N., Mickelson-Young, L. A., Atkinson, S. J., and Quilliam, L. A. (1999) *J. Biol. Chem. 274*, 4551−4560.
33. Walker, S. J., Wu, W. J., Cerione, R. A., and Brown, H. A. (2000) *J. Biol. Chem. 275*, 15665−15668.
34. Zong, H., Kaibuchi, K., and Quilliam, L. (2001) *Mol. Cell. Biol. 21*, 5287−5298.
35. McCallum, S. J., Wu, J. W., and Cerione, R. A. (1996) *J. Biol. Chem. 271*, 21732−21737.
36. Farnsworth, C. L., and Feig, L. A. (1991) *Mol. Cell. Biol. 11*, 4822−4829.
37. Hurley, J. H., and Misra, S. (2000) *Annu. Rev. Biophys. Biomol. Struct. 29*, 49−79.
38. Mott, H. R., Owen, D., Nietlispach, D., Lowe, P. N., Manser, E., Lim, L., and Laue, E. D. (1999) *Nature 399* (6734), 384−388.
39. Abdul-Manan, N., Aghazadeh, B., Liu, G. A., Majumdar, A., Ouerfelli, O., Siminovitch, K. A., and Rosen, M. K. (1999) *Nature 399* (6734), 379−383.
40. Zheng, Y., Bagrodia, S., Cerione, R. A. (1994) *J. Biol. Chem. 269* (29), 18727−18730.

BI0120087